# ROBUST CONTROL FOR A PNEUMATIC MUSCLE ACTUATOR SYSTEM

Liu-Hsu Lin[1], Jia-Yush Yen[2] and Fu-Cheng Wang[2]
[1]*Department of Mechanical Engineering, De Lin Institute of Technology, New Taipei City, Taiwan*
[2]*Department of Mechanical Engineering, National Taiwan University, Taipei, Taiwan*
*E-mail: lslin@dlit.edu.tw; jyen@ntu.edu.tw; fcw@ntu.edu.tw*

ICETI 2012-I1052_SCI
No. 13-CSME-44, E.I.C. Accession 3502

## ABSTRACT
This paper presents the modeling and robust control of a pneumatic muscle actuator system. Due to the inherent nonlinear and time-varying characteristics of this system, it is difficult to achieve excellent performance using conventional control methods. Therefore, we apply identification techniques to model the system as linear transfer functions and regard the un-modeled dynamics as system uncertainties. Because $H_\infty$ robust control is well-known for its capability in dealing with system uncertainties, we then apply $H_\infty$ robust control strategies to guarantee system stability and performance for the system. From the experimental results, the proposed $H_\infty$ robust controller is deemed effective.

**Keywords:** pneumatic muscle actuator; robust control; system identification.

# SYSTÈME D'IDENTIFICATION ET DE CONTRÔLE ROBUSTE D'UN SYSTÈME DE COMMANDE PNEUMATIQUE MUSCULAIRE

## RÉSUMÉ
Cet article présente la modélisation et la commande robuste d'un système de vérin pneumatique musculaire. En raison des caractéristiques inhérentes non-linéaires et, variant dans le temps de ce système, il est difficile d'atteindre d'excellentes performances en utilisant des méthodes de contrôle classiques. Par conséquent, nous appliquons des techniques d'identification afin de modéliser le système en tant que fonction de transfert linéaire et considérons la dynamique non-modélisés comme des incertitudes du système. Parce que la commande $H_\infty$ robuste est bien connue pour sa capacité à faire face aux incertitudes du système, nous avons ensuite appliqué des stratégies de contrôle $H_\infty$ robustes pour garantir la stabilité du système et ses performances. A partir des résultats expérimentaux, le contrôleur proposé $H_\infty$ robuste est jugé efficace.

**Mots-clés :** actionneur pneumatique musculaire ; commande robuste ; d'identification du système.

## 1. INTRODUCTION

Over the past decade, the pneumatic muscle (PM) has drawn much attention as a novel actuator, and it has been regarded as an alternative actuator to hydraulic and electric actuators because of its favorable characteristics such as a high power/weight ratio, a high power/volume ratio, low cost, compactness, ease of maintenance, cleanliness, inexpensive power source, and inherent safety. Owing to these advantages, the PM actuator can be applied not only in the industrial applications but also more popularly in bionic robots [1] and therapy devices [2, 3]. However, due to the inherent nonlinearity and the time-varying dynamics of the PM actuator system, it is still a challenge to develop a good control technique for the system. Therefore, many studies have proposed the linear or nonlinear control methods to achieve good control performance; for example, Bennett [4] and Caldwell [5] applied the PID control strategy to a PM actuator system. In [6, 7], the adaptive tracking controller was developed for a PM actuator output tracking. A self-organized fuzzy control was applied for angle control of a one-dimension pneumatic muscle arm in [8]. Harald [9] developed the sliding-mode control for manipulators driven by the PM actuators. However, the main problem of the sliding-mode control is chattering that can result in a high amount of control efforts. The aforementioned control methods are usually developed based on the assumptions of a linearized model, constant payload, and constant supply pressure. They cannot guarantee good control performance and stability for varying system conditions and external disturbances. On the other hand, the $H_\infty$ robust control is well-known for its capability in dealing with system uncertainties and external disturbances [11, 12]. Furthermore, the implementation of the $H_\infty$ robust control is much simpler than other advanced control strategies, such as adaptive control and gain scheduling control that both need to update parameters according to the responses of the system. Although in the past, many scientists [13, 14] have successfully developed $H_\infty$ robust controllers for different pneumatic systems such as pneumatic cylinders and air motors, very few research efforts have applied $H_\infty$ robust control to the PM actuator systems.

Therefore, we applied $H_\infty$ robust control strategies to a PM actuator system in this paper. First, we modeled the PM dynamics as a linearized transfer function with uncertainties. Then we designed a $H_\infty$ robust controller to guarantee system stability and performance. Finally, the proposed controller was implemented for experimental verification.

## 2. MODEL AND IDENTIFICATION

### 2.1. Dynamic Model of PM Actuator

In this section, we discuss the dynamics of a single pneumatic muscle, as shown in Fig. 1. The end of the pneumatic muscle is connected vertically with a mass. When internal pressure is applied, the hose expands in a peripheral direction, thus creating a tensile force and a contraction motion in the longitudinal direction. Using the force equilibrium theorem [14], the PM actuator can be simplified as a mathematical model with three elements: a nonlinear contractile element $Fc$, a nonlinear damper $B$, and a nonlinear spring $K$, as illustrated in Fig. 1(c)

By applying a constant weight $M$ to the end of the system, the dynamics of pneumatic muscle can be described as in the following equation:

$$M\ddot{y} + B(p)\dot{y} + K(p)y = Fc(p) - Mg, \tag{1}$$

where $y$ is the contraction length of the pneumatic muscle and $p$ is the pressure of the muscle. The following parameters are given in [15]:

$$Fc = 2.43P - 1.29 \times 10^{-3}P^2 \text{ (N)}, \tag{2}$$

$$K = 5.71 + 0.0307p \text{ (N/mm)}, \tag{3}$$

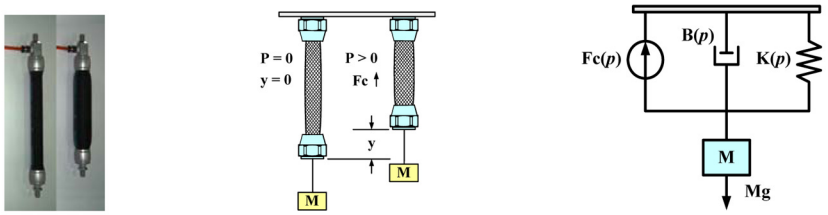


(a) (b) (c)

Fig. 1. The dynamics of a single pneumatic muscle: (a) component; (b) illustration; (c) model of a single pneumatic muscle.

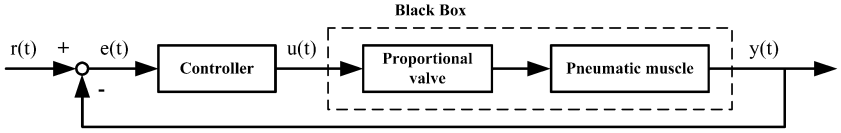


Fig. 2. Pneumatic muscle actuator system.

$$B = \left\{ \begin{array}{ll} 1.01 + 0.00691p & (\mathrm{N \cdot s/mm}), \quad \text{Inflation} \\ 0.6 - 0.000803p & (\mathrm{N \cdot s/mm}), \quad \text{Deflation} \end{array} \right\}. \tag{4}$$

We note that the model is nonlinear because of the $p^2$ term and $B(p)$. In addition, the model is derived based on a constant load and a constant pressure. Besides, the performance of the PM actuator system is affected not only by the pneumatic muscle but also by the proportional valve as shown in Fig. 2. Therefore, we consider the whole PM actuator system as a black box and apply the system identification method to obtain mathematical models of the PM system, as in the following.

### 2.2. System Identification

System transfer functions can be identified by analyzing the test input and output signals of the system. In this work, the Black-Box-Space Model is selected to identify the plant with batch data $[u(t), y(t)]$ [15]. The model of the PM actuator system is expressed as

$$x(t+Ts) = Ax(t) + Bu(t) + Ke(t), \tag{5}$$

$$y(t) = Cx(t) + Du(t) + e(t), \tag{6}$$

where $y(t)$ is the contractile length of the PM and $u(t)$ is the voltage input to the proportional valve. In order to simulate system characteristics at all frequencies, a pseudo random binary sequence (PRBS) was used as the input signal $u(t)$ for system identification. The PRBS signals that resemble pure white noise can be realized easily from a combination of a series of square waves of random time duration, such that the spectrum contains rich sinusoidal waves to excite all system dynamics. Considering the variations of external payload and supply pressure, nine experiments were carried out for three different payloads (2, 4, and 8 kg) with varying supply pressures (4.5, 5.0, and 5.5 bar). In this work, when $M = 4$ kg and $p = 5$ bar, the input and output signals for system identifications are shown in Fig. 3.

Comparing the input signal $u(t)$ and output signal $y(t)$, system identification was carried out as the following procedure:

1. The PRBS signal was given as input to operate the PM actuator to contract and expand randomly from 0–45 mm.

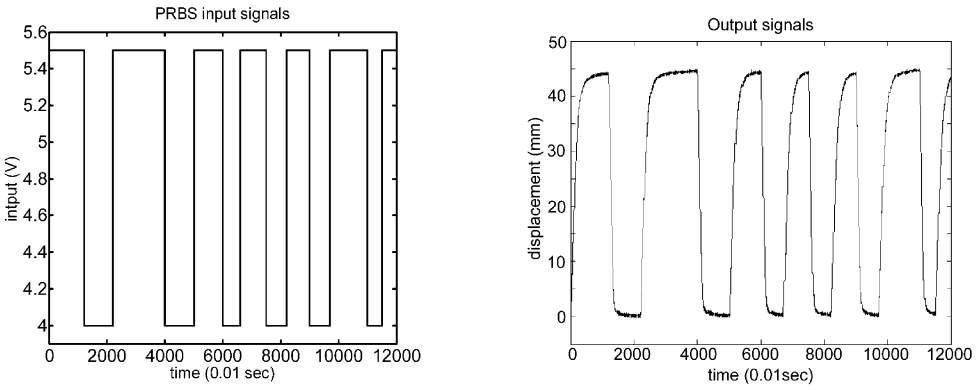


Fig. 3. Input and output signals of the PM system.

Table 1. Results of continuous-time system identification.

| | 2 kg loads | 4 kg loads | 8 kg loads |
|---|---|---|---|
| 4.5 bar | $G_1(s) = \frac{0.1691}{s+0.3641}$ | $G_2(s) = \frac{0.1464}{s+0.3376}$ | $G_3(s) = \frac{0.1307}{s+0.319}$ |
| 5 bar | $G_4(s) = \frac{0.1535}{s+0.3303}$ | $G_5(s) = \frac{0.1439}{s+0.326}$ | $G_6(s) = \frac{0.1362}{s+0.3307}$ |
| 5.5 bar | $G_7(s) = \frac{0.152}{s+0.3216}$ | $G_8(s) = \frac{0.1478}{s+0.3284}$ | $G_9(s) = \frac{0.1332}{s+0.3137}$ |

2. The input and output data was sampled with a sampling time of 0.01 seconds and were manipulated by the Matlab solver pem to calculate the system transfer functions as shown in Table 1.

3. The discrete time transfer functions were then transformed to continuous time by the zero order hold method, as illustrated in Table 1, in order to perform the robust controller design described in Section 4.

## 3. ROBUST CONTROLLER DESIGN

In this section, robust control strategies will be briefly introduced. By analyzing the robust stabilization and gap metrics for a left coprime factor (LCF) perturbed system [17], a robust controller will be designed to provide the maximum stability bound and achieve the precise tracking performance for the pneumatic muscle actuator system. The resulting controller will be verified by experiments in the next section.

### 3.1. Robust Stabilization for the LCF Plant

In this paper, we first linearize the PM actuator system and treat the residual nonlinear terms as system uncertainties. Then the PM actuator system can be represented as a left coprime factor perturbed system as shown in Fig. 4 and described as follows:

$$G_\Delta = (M + \Delta_M)^{-1}(N + \Delta_N), \tag{7}$$

where uncertainty $\Delta := [\Delta_M, \Delta_N]$, $\Delta_M, \Delta_N \in RH_\infty$. And the nominal plant $G_0$ can be defined as $G_0 := M^{-1}N$, in which $M, N \in RH_\infty$ and $MM^* + NN^* = I$ for all $\omega$. The closed-loop system transfer function can be simplified as follows:

$$\begin{bmatrix} u \\ y \end{bmatrix} = \begin{bmatrix} K \\ I \end{bmatrix} (I + G_0K)^{-1}M^{-1}\omega. \tag{8}$$

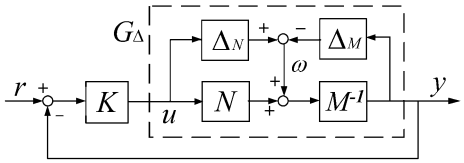


Fig. 4. Feedback structure of left coprime factor perturbed systems.

By the small gain theorem [17], the closed-loop system remains internally stable for all $\| [\Delta_M, \Delta_N] \|_\infty < \varepsilon$ if and only if

$$\left\| \begin{bmatrix} K \\ I \end{bmatrix} (I + G_0 K)^{-1} M^{-1} \right\|_\infty = \left\| \begin{bmatrix} K \\ I \end{bmatrix} (I + G_0 K)^{-1} \begin{bmatrix} I & G_0 \end{bmatrix} \right\|_\infty \leq 1/\varepsilon. \tag{9}$$

Thus, we can define the stability margin of the system as follows:

**Definition 1** (Stability Margin [16]). The stability margin of the closed-loop system is defined as

$$b(G_0, K) \equiv \left\| \begin{bmatrix} K \\ I \end{bmatrix} (I + G_0 K)^{-1} \begin{bmatrix} I & G_0 \end{bmatrix} \right\|_\infty^{-1}. \tag{10}$$

Hence, from small gain theorem the closed-loop system is internally stable for all $\| [\Delta_M, \Delta_N] \|_\infty < \varepsilon$ if and only if $b(G_0, K) \geq \varepsilon$. It is further noted that the coprime factor perturbed system is not unique. That is, there is more than one expression for $G_0$ or $G_\Delta$. Therefore, the gap between two systems $G_0$ and $G_\Delta$ can be defined as $\delta(G_0, G_\Delta)$.

**Definition 2** (Gap Metric [17]). The smallest value of $\| [\Delta_M, \Delta_N] \|_\infty$ which perturbs $G_0$ into $G_\Delta$, is called the gap between $G_0$ and $G_\Delta$ is denoted as $\delta(G_0, G_\Delta)$.

### 3.2. Selection of the Nominal Plant

From the definitions, $b(G_0, K)$ gives the radius (in terms of gap metrics) of the largest ball of plants stabilized by the controller $K$. Therefore, the goal of the controller design is to derive a suitable controller $K$ from a nominal plant $G_0$, such that all perturbed plants $G_i$ located inside the gap $\delta(G_0, G_i) < \varepsilon$ will satisfy $b(G_0, K) \geq \varepsilon$ and the closed-loop system will remain internally stable [17].

The selection of the nominal plants $G_0(s)$ was based on the calculation of gaps between the nominal plants and the perturbed plants, such that the maximum gap is minimized as

$$\min_{G_0} \max_{G_i} \delta(G_0, G_i). \tag{11}$$

Considering the system transfer functions in Table 1, the gaps between all plants are illustrated in Table 2. Therefore, $G_2$ was selected as the nominal plant because the maximum gap between $G_2$ and other plants is 0.0332, which is the minimum of all systems. That is,

$$G_0(s) = G_2(s) = \frac{0.1464}{s + 0.3376}, \tag{12}$$

such that $\delta(G_0, G_i) < 0.0332$ for all perturbed system $G_i$.

Table 2. Gaps between the system transfer functions.

| | $G_1$ | $G_2$ | $G_3$ | $G_4$ | $G_5$ | $G_6$ | $G_7$ | $G_8$ | $G_9$ |
|---|---|---|---|---|---|---|---|---|---|
| $G_1$ | 0 | **0.0332** | **0.0576** | 0.0205 | **0.0351** | 0.0507 | 0.0234 | 0.0293 | **0.0517** |
| $G_2$ | 0.0332 | 0 | 0.0254 | 0.0263 | 0.0068 | 0.0195 | 0.0332 | 0.0146 | 0.0195 |
| $G_3$ | **0.0576** | 0.0254 | 0 | **0.0468** | 0.0273 | 0.0088 | **0.0527** | **0.0341** | 0.0137 |
| $G_4$ | 0.0205 | 0.0263 | 0.0468 | 0 | 0.0195 | 0.0449 | 0.0068 | 0.0127 | 0.0361 |
| $G_5$ | 0.0351 | 0.0068 | 0.0273 | 0.0195 | 0 | 0.0254 | 0.0263 | 0.0078 | 0.0176 |
| $G_6$ | 0.0507 | 0.0195 | 0.0088 | 0.0449 | 0.0254 | 0 | 0.0517 | 0.0332 | 0.0117 |
| $G_7$ | 0.0234 | **0.0332** | 0.0527 | 0.0068 | 0.0263 | **0.0517** | 0 | 0.0195 | 0.04 |
| $G_8$ | 0.0293 | 0.0146 | 0.0341 | 0.0127 | 0.0078 | 0.0332 | 0.0195 | 0 | 0.0244 |
| $G_9$ | 0.0517 | 0.0195 | 0.0137 | 0.0361 | 0.0176 | 0.0117 | 0.04 | 0.0244 | 0 |
| **Max** | **0.0576** | **0.0332** | **0.0576** | **0.0468** | **0.0351** | **0.0517** | **0.0527** | **0.0341** | **0.0517** |

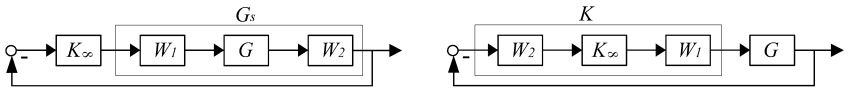


Fig. 5. Design procedures of robust controllers.

### 3.3. $H_\infty$ Loop-Shaping Design Procedure

The design procedures of robust controllers are illustrated as follows [18]:

1. Loop shaping design: Using a pre-compensator $W_1$ and a post-compensator $W_2$, the nominal plant $G$ is shaped to form a shaped plant $G_s = W_1 G W_2$, as shown in Fig. 5a

2. Robust stabilization estimate: The maximum stability margin $b_{\max}$ is defined as follows:

$$b_{\max}(G_s, K) = \inf_{K \text{ stabilizing}} \left\| \begin{bmatrix} K \\ I \end{bmatrix} (I + G_s K)^{-1} \begin{bmatrix} I & G_s \end{bmatrix} \right\|_\infty^{-1}, \tag{13}$$

   where $G_s = M_s^{-1} N_s$ and $M_s, N_s$ are the normalized left coprime factorization of $G_s$. If $b_{\max}(G_s, K) << 1$, then we must return to step Eqn. (1) and modify $W_1$ and $W_2$. Finally, we can select an $\varepsilon \leq b_{\max}(G_s, K)$ and synthesize a stabilizing controller $K_\infty$, which satisfies

$$\left\| \begin{bmatrix} K_\infty \\ I \end{bmatrix} (I + G_s K_\infty)^{-1} \begin{bmatrix} I & G_s \end{bmatrix} \right\|_\infty^{-1} \geq \varepsilon.$$

3. The designed controller $K_\infty$ is then multiplied by the weight functions, such that $K = W_1 K_\infty W_2$ is implemented to control the system $G$, as illustrated in Fig. 5b.

### 3.4. $H_\infty$ Robust Controller Design

Using the aforementioned design procedures with nominal plant $G_0$ from Eq. (12) and the following weighting functions:

$$W_1 = \frac{49.86}{s}, \quad W_2 = 1,$$

a $H_\infty$ robust controller can be designed as

$$K_{h\inf}(s) = \frac{-110.8s - 144}{s^2 + 6.383s}, \tag{14}$$

with stability margin $b(G_0, K_1) = 0.4112$, which is much bigger than the system perturbation $\delta(G_0, G_i) = 0.0332$. This controller will be implemented in Section 4 for performance analysis.

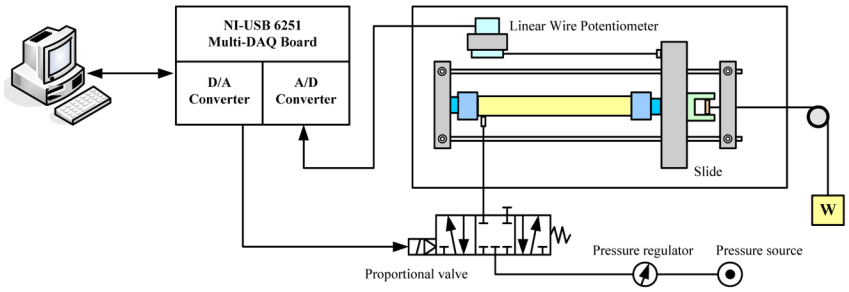


Fig. 6. Schematic diagram of the experimental apparatus.

## 4. EXPERIMENT AND RESULTS

### 4.1. Experimental Setup

In order to verify the performance of the proposed $H_\infty$ robust controller, a test platform driven by a pneumatic muscle actuator is constructed. The test platform consists of a slide mechanism. One side of the pneumatic muscle actuator is fixed to the base, while the other side is attached to a movable slide. The movable slide is connected to a loading weight by a steel cable. In this experimental setup, a personal computer calculates and transfers the control voltage signal to control the proportional valve through a multi-DAQ board. The linear displacement of the PM actuator is measured by a linear wire potentiometer and fed back to the computer through the multi-DAQ board. The external loading weight can be changed from 2 to 8 kg, which is a 400% variation with respect to the minimum loading weight condition. Besides, the experiment is conducted with the varying pressure of 3.0–5.5 bar. The nominal supply pressure is 5 bar. The schematic diagram of the experimental apparatus is shown in Fig. 6.

### 4.2. Experimental Results

In order to evaluate the effectiveness and robustness of the designed $H_\infty$ robust position controller, the following experiments were carried out. Furthermore, the experimental results were compared with those of a conventional PID controller $K_{\mathrm{PID}}(s) = (0.216s^2 + 21.73s + 7.326)/s$ designed by the Ziegler–Nichols method.

**Case 1: Position control performance test** To investigate the position control performance of the proposed controller, the experiments were carried out with three different step reference inputs (10 mm, 20 mm and 30 mm) under a constant loading weight $W = 4$ kg. The initial position of the weight is 0 mm, when the PM is fully deflated and extended. The step responses of the proposed controller and the conventional PID controller are shown in Fig. 7. Furthermore, to quantify the system performance, the root-mean-square (RMS) tracking error is defined as follows:

$$\text{RMS tracking error} = \left( \frac{\sum_{i=1}^{N-1} (y_{i+1} - r_i)^2}{N-1} \right)^{1/2}, \tag{15}$$

in which $N$ is the number of sampling points. In view of the steady response and the repeatability of system, we selected $N = 1200$ in Case 1, and $N = 12000$ in Cases 2 and 3. The system performances of the aforementioned two controllers at different operating points are numerically listed in Table 3. As shown in Fig. 7, the experimental results show that the robust controller $K_{h\inf}$ achieves better position control than the PID controller $K_{\mathrm{PID}}$ at all operating points. In addition, the settling time of the robust controller $K_{h\inf}$ is much shorter than that of the PID controller $K_{\mathrm{PID}}$.

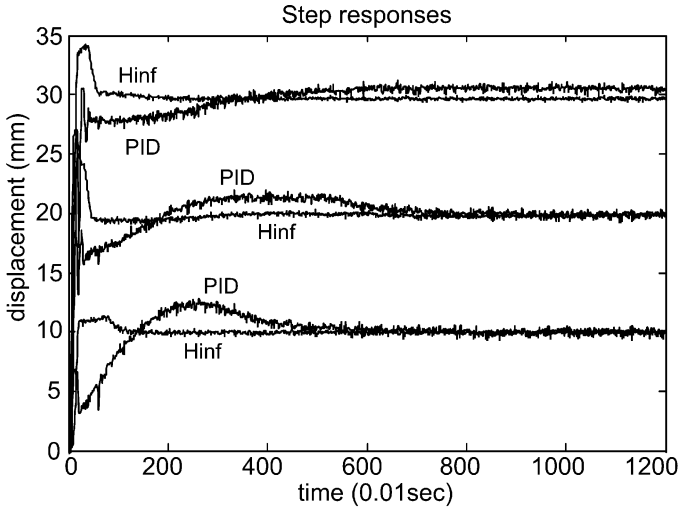


Fig. 7. Step responses of the controller $K_{h\inf}$ and $K_{\mathrm{PID}}$.

Table 3. RMS tracking errors of the two controllers at different operating points.

| | Reference inputs (10 mm) | Reference inputs (20 mm) | Reference inputs (30 mm) |
|---|---|---|---|
| $K_{h\inf}$ | 0.16 mm | 0.16 mm | 0.19 mm |
| $K_{\mathrm{PID}}$ | 0.23 mm | 0.23 mm | 0.39 mm |

Table 4. RMS tracking errors of the two controllers with different mass loads.

| | Mass load : 2 kg | Mass load : 4 kg | Mass load : 8 kg |
|---|---|---|---|
| $K_{h\inf}$ | 0.16 mm | 0.18 mm | 0.19 mm |
| $K_{\mathrm{PID}}$ | 0.3 mm | 0.32 mm | 0.41 mm |

**Case 2: Robustness test with different loading weights** In practical applications, the loading weight will be changed. To verify the robustness of the proposed controller to the loading variations, the experiments were carried out with a square wave reference input corresponding to three different loading weights of 2, 4, and 8 kg. The comparison between the proposed controller and the conventional PID controller is presented in Fig. 8 and Table 4. It can be seen that the proposed controller has superior robust performance for a PM actuator system with loading uncertainties.

**Case 3: Robustness test with different supply pressures** Similarly, we tested the robustness of the PM actuator system with pressure uncertainties. The tracking responses of the sinusoidal wave reference input with three different supply pressures: 3.0 bar, 4.5 bar, and 5.5 bar are shown in Fig. 9. The RMS tracking errors are numerically listed in Table 5. From the experimental results of the Cases 2 and 3, it can be seen that the tracking error of the proposed controller is less than 0.2 mm, which compared with the maximum stroke that is less than 1%. It indicates that the proposed controller has superior robust performance for a PM system against the pressure uncertainty and external load variation.

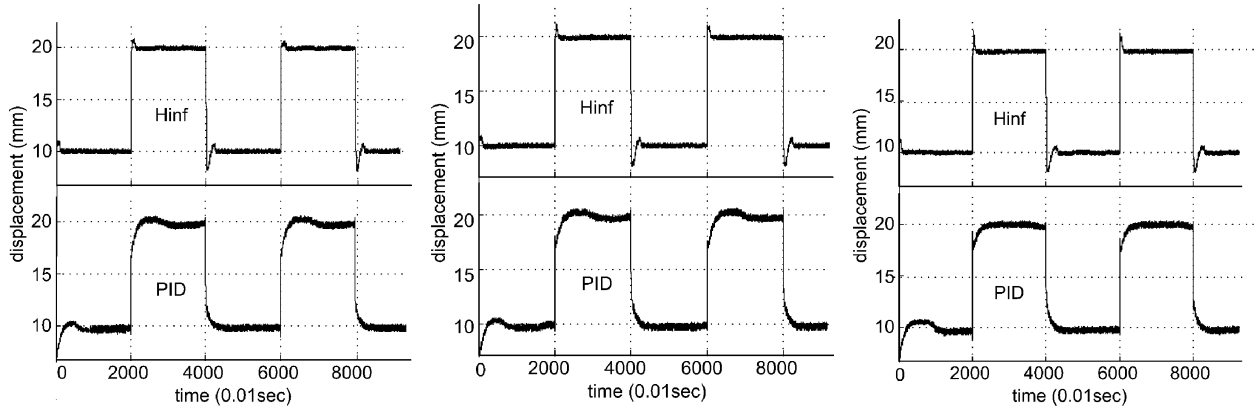


Fig. 8. Experimental results with different loading weights: (a) 2 kg load; (b) 4 kg load; (c) 8 kg load.

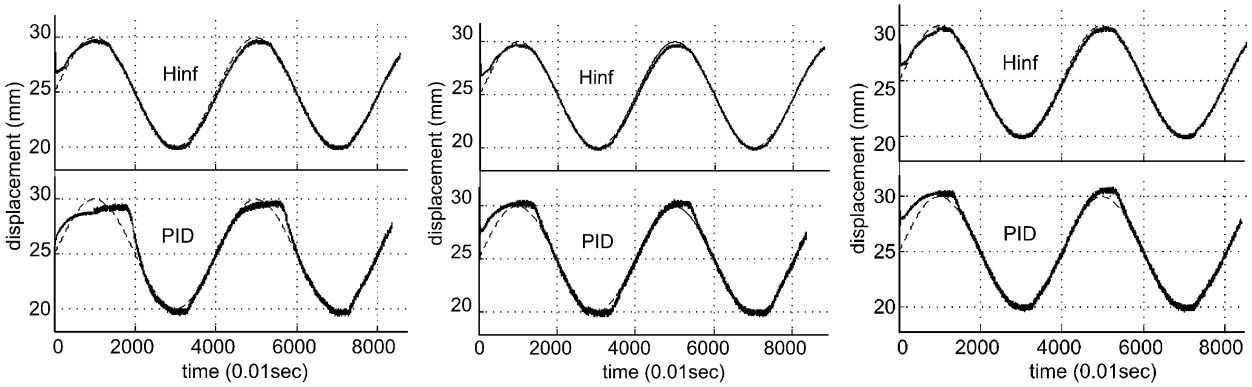


Fig. 9. Experimental results with different supply pressures: (a) P = 3 bar; (b) P = 4.5 bar; (c) P = 5.5 bar.

Table 5. RMS tracking errors of the two controllers with different supply pressures.

| | supply pressure: 3.0 bar | supply pressure: 4.5 bar | supply pressure: 5.5 bar |
|---|---|---|---|
| $K_{h\inf}$ | 0.20 mm | 0.18 mm | 0.17 mm |
| $K_{\mathrm{PID}}$ | 0.46 mm | 0.28 mm | 0.21 mm |

## 5. CONCLUSIONS

This paper has applied system identification and robust control for a pneumatic muscle actuator system. From system identification, the pneumatic muscle actuator system was modeled as a linear system. By selecting the nominal plant, the system variations were regarded as system uncertainties and disturbances that can be treated by the proposed robust controller. Using the weighting function, a $H_\infty$ robust position controller was designed to improve system stability and performance. Then the designed robust controller was implemented for experimental verifications. From the results, the proposed controller can achieved robust performance for varying system conditions and external disturbances. In the future, the proposed control strategies can be practically implemented for therapy devices with pneumatic muscle actuators.

## REFERENCES

1. Information on http://www.festo.com/bionic, Bionic projects in the technical automation.

2. Xing, K., Xu, Q., He, J., Wang, Y., Liu, Z. and Huang, X., "A wearable device for repetitive hand therapy", in *Proceedings of the 2nd Biennial IEEE/RAS-EMBS International Conference on Biomedical Robotics and Biomechatronics*, Scottsdale, AZ, USA, pp. 919–923, Oct. 19–22, 2008.
3. Balasubramanian, S., Wei, R. and He, J., "RUPERT: Closed loop control design", in *Proceedings 30th IEEE/EMBS Annual International Conference*, Vancouver, Canada, pp. 3467–3470, Aug. 20–25, 2008.
4. Bennett, S., "Development of the PID controller", *Control Systems Magazine in IEEE*, Vol. 13, No. 6, pp. 58–62, 1993.
5. Caldwell, D.G., Medrano-Cerda, G.A. and Goodwin, M.J., "Braided pneumatic actuator control of a multi-jointed manipulator", in *Proceedings IEEE International Conference on Systems, Man and Cybernetics*, Noesis, Velizy, France, pp. 423–428, Oct. 17–20, 1993.
6. Lilly, J., "Adaptive tracking for pneumatic muscle actuators in bicep and tricep configurations", *IEEE Transactions on Neural Systems and Rehabilitation Engineering*, Vol. 11, No. 3, pp. 333–339, 2003.
7. Medrano-Cerda, G.A., Bowler, C.J. and Galdwell, D.G., "Adaptive position control of antagonistic pneumatic muscle actuators", In *Proceedings of Intelligent Robost and Systems IEEE International Conference*, pp. 378–383, Aug. 5–9, 1995.
8. Ming-kung Chang, Ping-Lang Yen and Tsan-hsiu Yuan, "Angle control of a one-dimension pneumatic muscle arm using self-organizing fuzzy control", *System, Man and Cybernetics IEEE Int. Conf.*, Taipei, Taiwan, pp. 3834–3838, Oct. 8–11, 2006.
9. Harald, A. and Dominik, S., "Sliding-mode control of a high-speed linear axis driven by pneumatic muscle actuator", *IEEE Transactions on Industrial Electronics*, Vol. 55, No. 11, pp. 3855–3864, 2008.
10. Zhon, K., Doyle, J.C. and Glover, K., *Robust and Optimal Control*, Prentice-Hall, New Jersey, 1996.
11. Maciejowski, J.M., *Multivariable Feedback Design*, Addison Wesley, 1990.
12. Kaitwanidvilai, S. and Parnichkun, M., "Genetic-algorithm-based fixed-structure robust H8 loop-shaping control of a pneumatic servo system", *Journal of Robotics and Mechatronics*, Vol. 16, No. 4, pp. 362–373, 2004.
13. Lin, L. and Yen, J., "Dynamic modeling and robust controller design for air motor", in *Proceedings of the 27th Chinese Control Conference IEEE*, Yunnan, China, pp. 748–752, July 16–18, 2008.
14. Reynolds, D.B., Reynolds, D.W., Repperger, D.W., Phillips, C.A. and Bandry, G., "Modeling the dynamic characteristics of pneumatic muscle", *Annals of Biomedical Engineering*, Vol. 31, No. 3, pp. 310–317, 2003.
15. Ljung, L., *System Identification Theory for the User*, 2nd ed., Prentice Hall, New Jersey, 1999.
16. Zhou, K. and Doyle, J.C., *Essentials of Robust Control*, Prentice-Hall, New Jersey, 1998.
17. Georgiou, T.T. and Smith, M.C., "Optimal robustness in gap metric", *IEEE Transactions on Automatic Control*, Vol. 35, pp. 673–686, 1990.
18. McFarlane, D. and Glover, K., "A loop shaping design procedure using synthesis", *IEEE Transactions on Automatic Control*, Vol. 37, pp. 759–769, 1992.